

# ANALYSIS OF BUILT-UP CLASSES IN URBANISED ZONES USING RADAR IMAGES

JOANNA PLUTO-KOSSAKOWSKA , JOANNA GICZAN 

Department of Photogrammetry, Remote Sensing and GIS, Warsaw University of Technology, Warsaw, Poland

Manuscript received: January 3, 2023

Revised version: April 26, 2023

PLUTO-KOSSAKOWSKA J., GICZAN J., 2023. Analysis of built-up classes in urbanised zones using radar images. *Quaestiones Geographicae* 42(3), Bogucki Wydawnictwo Naukowe, Poznan, pp. 195–211. 8 figs, 6 tables.

**ABSTRACT:** This paper presents the results of a study to determine the potential of radar imaging to detect classes of built-up areas defined in the Urban Atlas (UA) spatial database. The classes are distinguished by function and building density. In addition to the reflectance value itself, characteristics such as building density or spatial layout can improve the identification of these classes. In order to increase the classification possibilities and better exploit the potential of radar imagery, a grey-level co-occurrence matrix (GLCM) was generated to analyse the texture of built-up classes. Two types of synthetic-aperture radar (SAR) images from different sensors were used as test data: Sentinel-1 and ICEYE, which were selected for their different setup configurations and parameters. Classification was carried out using the Random Forests (RF) and Minimum Distance (MD) methods. The use of the MD classifier resulted in an overall accuracy of 64% and 51% for Sentinel-1 and ICEYE, respectively. In ICEYE, individual objects (e.g. buildings) are better recognised than classes defined by their function or density, as in UA classes. Sentinel-1 performed better than ICEYE, with its texture images better complementing the features of urban area classes. This remains a significant challenge due to the complexity of urban areas in defining and characterising urban area classes. Automatic acquisition of training fields directly from UA is problematic and it is therefore advisable to independently obtain reference data for built-up area categories.

**KEY WORDS:** urban area, texture analysis, GLCM, supervised classification, Urban Atlas

*Corresponding author: Joanna Pluto-Kossakowska, [joanna.kossakowska@pw.edu.pl](mailto:joanna.kossakowska@pw.edu.pl)*

## Introduction

Urban development can be structured, as an expression of rational urban policy, or uncontrolled, leading to chaotic suburbanisation, i.e. haphazard development and dispersed location of buildings. These encourage spatial chaos and have a negative impact on the landscape. Economic, social and environmental factors related to the municipality's own tasks are relevant here. The costs are borne by the municipalities in the area of the extensive development of technical infrastructure brought in after the investment

is made or those associated with transport, long distances to work and services and negative environmental impacts. In order to counteract the above-mentioned impacts, efforts are being made to reuse urban space and move towards a compact city structure (Denis 2018).

Remote sensing images can capture the changes in urban areas but besides just visual observations it also can provide quantification and more detailed information on the impacts of those changes (SDG 2015). Built-up density maps can provide valuable additional information for assessing population distribution within the

urban area (Molch 2009, GHSL 2022). Accessible and widely used satellite optical data, although intuitive and commonly applied, have their limitations. Radar data, which are more difficult to interpret, require additional pre-processing and appropriate software. However, urban mapping can benefit from this type of data since built-up structures induce strong backscatter and thus can be distinguished well on radar imagery (Molch 2009). The different scattering effects on anthropogenic objects, including buildings, roads or other impervious surfaces, make these surfaces identifiable and distinguishable. In addition, the speckle effect, which gives the impression of noise, is an accumulation of many scattering mechanisms, but in reality it is systematic (Braun and Saulgau 2019). These speckles appear even when the object being imaged is relatively smooth and homogeneous. It is the effect of the coherent nature of the emitted radar signal (Goodman 1976).

The imaging of buildings on radar imagery depends on the orientation of the buildings to the direction of incidence of the microwave beam. Buildings that are oriented in a different direction than perpendicular can be mapped weaker due to the reflection from their walls. Back scattering also depends on the type of building – in the case of residential buildings, the value of recorded reflected radiation is the lowest, whereas it is higher for commercial areas and highest for industrial buildings (Eckardt et al. 2021).

Regular and repetitive features of the surface of the object are represented by the texture that determines the degree of regularity in a model (Snitkowska 2004). Some studies have reported that synthetic-aperture radar (SAR) texture imagery improves land cover mapping (Dell'Acqua, Gamba 2003). Kamusoko (2022) increased classification results on urban area from 0.66 to 0.83 of  $\kappa$  using additional texture indices. Adding texture measures to the classification improves its result, because it allows description of spatial relations, as a certain structure (Hall-Beyer 2017a).

There are many different methods for texture analysis, e.g. fractal analysis, discrete wavelet transform, Laplace filters, Markov random fields or granulometric analysis (Kupidura 2015). Studies show their potential in building detection and extraction in the automatic process,

but mainly in very high-resolution optical images, e.g. through a set of morphological operators (Kupidura and Uwarowa 2017, Huang and Zhang 2020). These approaches are also popular for land cover classification in optical images of different resolutions (Lewiński, Aleksandrowicz 2012, Kupidura 2019).

An effective tool for examining texture in digital images is the grey-level co-occurrence matrix (GLCM), which shows how often given combinations of reference and adjacent pixel values occur in an image (Zhang, Wang 2001). Many statistical texture measures can be calculated using a GLCM. Most of them were standardised by Haralick et al. (1973), who proposed 14 different measures. GLCM is a versatile tool because it allows measurement of roughness and directionality in one computation process. The GLCM counts the occurrences of pairs of pixel brightness values in a given direction. Most texture measures are weighted averages of the normalised GLCM matrix. Texture measures are divided into three groups: contrast, order and descriptive statistics (Hall-Beyer 2017a). A contrast group contains contrast-related measures; weights are based on the distance from the main diagonal. This group includes the following measures: Contrast, Dissimilarity and Homogeneity. Contrast measures significant changes in grey levels between adjacent pixels. Dissimilarity is visually similar to contrast; instead of weighing elements exponentially, the dissimilarity grows linearly when moving away from the main diagonal. The range of values will be different for these variables, but they contain essentially the same information. Homogeneity is sensitive to the presence of near-diagonal elements in GLCM, representing grey-level similarity between adjacent pixels (Hall-Beyer 2017a).

The ordering group contains the following measures: Angular Second Moment (ASM), Energy, MAX and Entropy, which cover the regularity of differences in pixel values occurring in a given window. The values of ASM are high when the pixels in a window are ordered or when the pixels are very similar (Mohanaiah et al. 2013). Energy is the square root of ASM and shows that the larger the order in the window, the greater its value; it is the opposite of entropy and measures texture uniformity. Maximum probability (MAX) is a measure of finding the

highest probability value in the GLCM matrix and is rarely implemented in programs for image processing. Entropy is a zero-degree measure. The greater the entropy, the greater the disorder or complexity in terms of texture (Hall-Beyer 2017b).

The descriptive statistics group of the GLCM matrix contains such variables as Mean, Variance and Correlation. GLCM Mean represents the product of the pixel value and frequency of occurrence in combination with a value of an adjacent pixel, the average value of grey levels in an image (Herold et al. 2003). GLCM Variance is a measure of heterogeneity that is based on the mean and the scattering of pixel values in the GLCM matrix around the mean. Variance is similar to contrast and dissimilarity. GLCM Correlation measures the linear dependence of grey levels on the values of adjacent pixels; its high value indicates the high predictability of pixel relation. For example, high pixel values tend to cluster with high values, whereas low pixel values with low values (Park and Guldman 2020). Nearby pixels are typically more correlated with each other than more distant pixels, and thus smaller window sizes will have a higher correlation than larger windows.

Texture images are the result of second-order calculations, which means that they consider the relationship between two categories of pixels, namely reference and adjacent pixels. Research shows that individual fragments of land cover have a higher correlation within their boundaries than between neighbouring objects (Hall-Beyer 2017b). For a comprehensive review on statistical algorithms and mathematical formulations, one can refer Haralick et al. (1973) and Hall-Beyer (2017a). Texture measures formulated in this way can be used as additional information for spatial structures analysis in urbanised areas and for distinguishing land cover classes in satellite images.

### Texture analysis in urban area

A feature of urban and suburban landscapes consists of a mosaic of heterogeneous types of land cover. They are characterised by high spectral variability, which makes it difficult to perform an accurate classification of land cover (Park and Guldman 2020). It is worth looking for other variables for classification that consider other

properties such as the neighbourhood. Wellmann et al. (2018) used GLCM at the parcel level to infer different degrees of land use intensity and seasonal variations within different urban plots. GLCM variance and contrast indicators provide the best variability to identify different land uses, with heavily developed surfaces showing no variability (Wellmann et al. 2018). Giannini et al. (2012) used principal component analysis executed on texture images that were obtained using QuickBird image. The selected Principal Component (PC) bands, in conjunction with the original panchromatic image, are classified using an object-based approach to categorise pixels into three classes: buildings, roads and vegetation. This study has shown that the best result can be achieved considering the several textural groups separately: Contrast, Orderliness and Statistic with  $\kappa$  of 91% (Giannini et al. 2012).

Radar data is used in the mapping of urban areas, mainly for the study of urban footprint. The examples of classification of built-up area on radar images described so far in the literature consisted mainly of the distinction between buildings and non-buildings (Semenzato et al. 2020). In research on the extraction of built-up areas in two cities (Wrocław and Kluź-Napoka), Iso-Tex and texture analysis were used on Sentinel-1 images (Holobăcă et al. 2019). The classification included images of backscatter obtained from descending and ascending orbits, images of speckles divergence and three components of GLCM (Energy, Mean and Variance) as input layers. Better results were obtained from unsupervised classification (ISODATA), and classes were aggregated into three classes: buildings, non-buildings and mixed. Thresholding was performed for the mixed class, and accuracies above 90% were achieved. The biggest differences between the buildings and other areas occurred in the images of Variance and Energy (Holobăcă et al. 2019).

Finding the best combination of texture images for the classification of the urban environment was the aim of a study conducted in the city of Lucknow (Pathak, Dikshit 2010). A division into 10 classes of land use and cover was established: 5 anthropogenic related to buildings and 5 nature-related. Texture images of GLCM Mean, Variance, ASM, Contrast and Entropy in five different randomly generated window sizes (from 5 to 21 pixels) were created. Four quantisation

levels (32, 64, 128 and 256) as well as four optical image channels (Red, Green, near and short infrared) were included. Out of 400 possible combinations arising as a result of applying Principal Component Analysis (PCA), the best 25 variants were selected. The results indicate that the choices of texture feature and window size have higher relative importance in the classification process than quantisation level or the choice of image band for extracting texture feature. The mean variable turned out to be the most important of the five analysed features (Pathak, Dikshit 2010).

Another example of using GLCMs concerns the detection of refugee camps based on optical and radar images (Braun and Hochschild 2015). The original texture of the Sentinel-1 images without removing the spots was used. GLCM derivatives were generated: Contrast, Correlation, Variance and Energy with different window sizes (3, 5 and 9). The Digital Elevation Model (DEM) from the Shuttle Radar Topography Mission (SRTM) was also used. PCA was performed, limiting the 26-element space features of Sentinel-1 to 7 elements, which allowed expediting the calculations. The area was classified by the Random Forests (RF) algorithm into 10 land cover classes. A higher number of input layers did not always result in higher accuracy. Furthermore, the study of data significance proved that radar data contributed only 20% to the final result, optical data 49% and DEM data 31%. Nevertheless, radar data helped to recognise classes that are similar in optical images - distinguishing between classes of vegetation or refugee camps and floodplains (Braun and Hochschild 2015).

Selected GLCM matrix parameters were also studied by Clausi (2002). The Contrast, Dissimilarity and Correlation variables gave very good classification results for all datasets. All three variables give consistent results for quantisation levels above 24. To create a complete set of features, the following should be selected: one statistic from the contrast group, one from the ordering group and correlation. Selecting more than one statistic (Contrast) always improves the result, although selecting all eight variables gave a weaker classification result than selection of the top three. The most used texture images are: Mean, Contrast, Entropy, Energy and Variance (Clausi 2002). Yoshioka et al. (2008) indicated the

Energy, Entropy, Homogeneity, Variance and Mean as the texture features selected to reduce the learning time in Support Vector Machine (SVM) classification with the same effectiveness in results shown by simulation. Kamusoko (2022) improved the RF classification of land cover by implementing texture (Variance, Mean) derived from multi-seasonal Sentinel-1 and Sentinel-2 images.

The other research of dividing the image content into two texture classes showed better results on the basis of transformations made with the Laplacian filter, and then with the Sobel, Sigma and PanBF filters. Compared to them, the usefulness of the Haralick function turned out to be smaller. The presented results find practical application in the work on the selection of appropriate classification algorithms for satellite images (Lewiński, Aleksandrowicz 2012). This review shows that many studies of built-up areas have been carried out on textures derived from optical images but rarely on those from SAR images. Furthermore, the GLCM tool allows the simultaneous generation of multiple texture images characterising different aspects and spatial relationships between objects. Hence, it appears to be a convenient and efficient tool. It is worth exploring the potential of texture on radar images to study urban morphology and structure.

### **The goal and scope of the research**

Assessing the compactness of a city's structure and analysing the density of buildings is very important in the context of the city's morphology and urban compactness (Denis 2018). The elements of a compact city can be understood as the physical presence of grey infrastructure objects and thus the proportion of non-permeable surfaces. This includes built-up areas, traffic routes, industrial areas or other areas covered with artificial materials. This study aims to assess the applicability of radar imagery and its texture images in urban zone classification and built-up area density assessment using the Urban Atlas (UA) database. The study used radar images acquired from two Sentinel-1 and ICEYE systems with different imaging parameters. Supervised classification was performed using synthetically produced texture images and the results were compared between sensors and to the UA database.

## Methods

Most of the research used digital classification (supervised or unsupervised) to distinguish classes or features in an urban area. In supervised classification with training dataset, there are diverse approaches, recognised as parametric e.g. Maximum Likelihood (ML), Minimum Distance (MD); or non-parametric e.g. RF or SVM (Richards 2013). There are advantages and disadvantages to using either, but there is no recommendation in the literature on which is better in which case. Many experiments have found a rather small or even no relationship between the algorithm and the results (Chen 2008). However, in case of multisource or multicategory data, more often ensemble methods are used. Ensemble classification methods train several classifiers and combine their results through a voting process e.g. RF (Joelsson et al. 2008). A RF is a collection of classification trees or treelike classifiers. Each tree gives a classification and the forest would have chosen the class having the most votes (Breinman 2001). Since this research is designed to check texture imagery input, MD as parametric (Richards 2013) and RF as ensemble method (Breinman, Cutler 2021) were selected for comparison of the results in this investigation. Both are recognised as simpler, less

computationally demanding and not-sensitive to noise classifiers (Joelsson et al. 2008, Kamusoko 2022).

In this research, an attempt is made to classify built-up areas defined according to the density of grey infrastructure and partly based on their function. It is assumed that GLCM and the generated texture images represent the variation in radar images and, therefore, allow distinguishing between built-up area classes in terms of type and density. It is also assumed that textured images represent the spatial characteristics of the classes described in the UA database. Built-up area classes in UA are distinguished based on the density of buildings, continuity and spatial arrangement. Thus, there is a chance that the above-mentioned features are reflected in the images derived from the GLCM matrix and will be a good foundation for classification allowing to differentiate the classes.

## Test area and UA database

Gdynia city (Poland), a port city located on the Baltic Sea, in the Pomeranian province and part of a common agglomeration (Trójmiasto), was chosen for the present research. It has an area exceeding 135 km<sup>2</sup>, with forests occupying 46% of the city's area, agricultural land 14%,

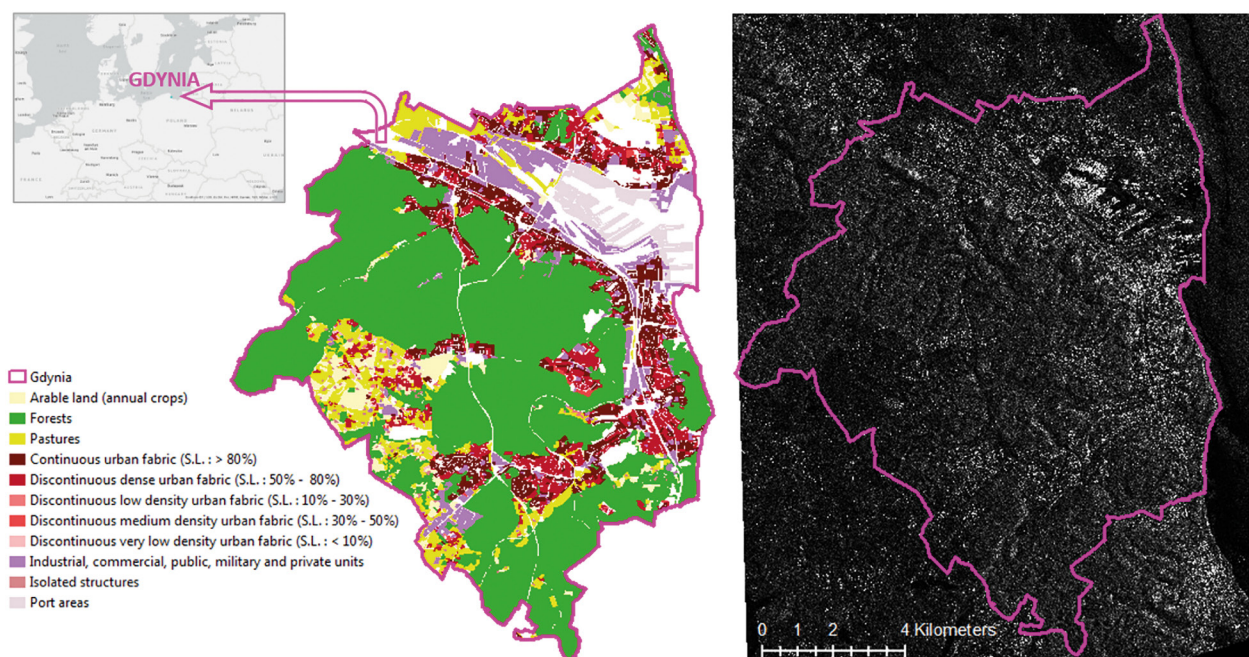


Fig. 1. The extent of Gdynia's boundary (purple lines) on the VV ICEYE image (right) and the visualisation of the UA database in the study area according to the UA legend (left). UA, Urban Atlas.

communication area 11%, residential areas 11%, industrial areas 5% and others 13% (BIP 2021). Gdynia is an area with diverse land use and according to the UA database (<https://land.copernicus.eu/local/urban-atlas>) there are 22 classes, including 8 built-up area classes described by Sealed Level (SL): Continuous urban fabric (CUF) (SL >80%), Discontinuous dense urban fabric (SL 50–80%), Discontinuous medium density urban fabric (DMDUF) (SL 30–50%), Discontinuous low density urban fabric (DLDUF) (SL 10–30%), Discontinuous very low density urban fabric (SL <10%), Isolated structures, Industrial, commercial, public, military and private units (ICPMAPU) and Port areas (PAs), and additionally, Arable land, Pastures and Forests (Fig. 1). The UA database is based on photo interpretation methodology using very high resolution images (mainly SPOT). Its geometrical and thematic accuracy refers to a scale of 1:10,000 and is dated 2018.

### Imagery data

Two types of radar imagery differing in wavelength and polarisation were selected for research – ICEYE and Sentinel-1 imagery. The ICEYE scene was acquired on 19 April 2019 and was made available in SLC format. The image was obtained in the Stripmap (SM) mode in the X band with a wavelength of 3 cm, which results in the spatial resolution of the intensity image of 2 m after corrections. ICEYE images are obtained in VV polarisation, with an ascending satellite orbit (Table 1). The Sentinel-1 satellite scene was acquired on 27 December 2018 by the Sentinel-1B satellite using the Interferometric Wide (IW) Swath mode in the C band with a wavelength of 5 cm in two polarisations (VH + VV). After resampling, an image of intensity with a spatial resolution of 10 m was obtained, and it was in the descending orbit. The years 2018 and 2019 were chosen considering the date of the latest updates to the UA to be consistent with this database frame (Urban Atlas, accessed 2 March 2021).

A different spatial resolution of the intensity images is obtained when recording the reflection of different wavelengths (C and X). For the C band (Sentinel-1) it is about 10 m after resampling, and for the X band (ICEYE) about 2 m. Thus, on the images themselves and their derivatives, it is possible to identify objects with different detail and different reflectivity characteristics.

### Processing and analysis

The Sentinel-1 satellite scene as a Ground Range Detected (GRD) product was downloaded from the CREODIAS Finder website, whereas ICEYE in SLC format was available at the ICEYE website. The first step of pre-processing for both images included radiometric calibration and topographic correction, as well as cropping the scene to the study area to reduce the data volume and processing time. The next step was to generate a GLCM, resulting in 10 derived images for each polarisation and sensor. Then the feature space was created, which consists of generated texture images and sigma zero ( $\sigma_0$ ) backscatter images.

From the available UA database, reference polygons were selected representing built-up area classes, defined in the UA, as well as three land cover classes – forests, pastures and farmlands – to maintain the continuity of land cover. For both radar images, the training fields were the same. Statistics have been calculated and a catalogue of objects has been created for the reference polygons. The catalogue provides an overview of built-up area classes and presents their similarity as well as diversity in texture images and backscatter images. It also allows identification of images that are similar or different for a given built-up area class. It can also help in selecting important variables for classification.

Afterwards, the classification was carried out supervised by two methods – RF with parameter change and MD. The RF algorithm allows an integration of data pertaining to different resolutions and from different sources. In addition,

Table 1. Specification of the SAR data used in the study.

Sensor	Date	Band	Polarisation	Orbit	Mode	Spatial resolution after corrections and resampling
ICEYE	19.04.2019	X (3 cm)	VV	Ascending	SM	2 m
Sentinel-1	27.12.2018	C (5 cm)	VH + VV	Descending	IW	10 m

the algorithm creates many different and uncorrelated classification and regression trees. The first RF classification attempt allowed identification of variables important in the classification and rejection of variables that were irrelevant or had a negative impact on the classification result. An assessment of the accuracy of the classification within the test polygons was carried out on 2000 points. The accuracies of the producer (P\_Accuracy) and the user (U\_Accuracy) of individual classes, as well as the total accuracy of the classification with the value of the *kappa* coefficient, were calculated in the assessment process. The obtained accuracies were the reason for the aggregation of 11 original classes into the following 4: dense urban area, low density urban area, industrial area and vegetation (Table 2).

A subset of the test fields was used to create a verification mechanism. The share of individual classes in a selected subset of test polygons was calculated, based on the image with aggregated classes. Using Python, a function was developed, which, based on the percentage of each class in each polygon, assigned the appropriate class name or marked the polygon for verification. To verify the algorithm, assignment statistics were calculated for a set consisting of 101 polygons, where, after an automatic verification process, a visual verification of the results was carried out.

Subsequently, the entire verification process was executed for the entire set consisting of 1750 polygons. The images analysis processes were carried out using SNAP (9.0.0), ArcMap (10.7.1), ArcGIS Pro (2.8.1) and Excel (ver. 2208) software tools.

## Results

The UA database contains 27 classes of land cover and land use. Eight classes of built-up areas and three classes of land cover/land use representing agriculture and forest were selected (Table 2). Percentage ranges of impermeable surfaces (SL) were determined according to the UA specification for the first five classes and were used for built-up areas' definition for classification.

The built-up area class polygons defined in the UA database served as training data in the classification. Their analysis and selection were carried out using an aerial orthophotomap from 2018 obtained from the National Geoportal ([geoportal.gov.pl](http://geoportal.gov.pl), accessed March 2021). Both the classification itself and the assessment of the accuracy were performed on the original UA polygons without any modifications. Table 2 shows the legend with class codenames used for all visualisation results included in this paper.

Table 2. Urban Atlas classes selected for the study. These code names and colours have been used in the forthcoming presentation of results.

Class name	Sealed Level (SL)	Codename and colour on images	Name and colour of aggregated classes
Continuous urban fabric	>80%	 CUF	 Dense urban area
Discontinuous dense urban fabric	50-80%	 DDUF	
Discontinuous medium density urban fabric	30-50%	 DMDUF	
Discontinuous low density urban fabric	10-30%	 DLDUF	 Low density urban area
Discontinuous very low density urban fabric	<10%	 DVLDUF	
Isolated structures		 IS	
Port areas		 PA	 Industrial area
Industrial, commercial, public, military and private units		 ICPMAPU	
Arable land (annual crops)		 AL	 Vegetation
Forests		 F	
Pastures		 P	
UA class borders			

## Sentinel-1

The Sentinel-1 satellite scene was subjected to radiometric calibration to the  $\sigma_0$  intensity image ( $\sigma_0$ ). In the next step, to facilitate the analysis of data from different sources, a topographic correction was performed to the Universal Transverse Mercator (UTM) cartographic system using SRTM (3s). A filtration step is often performed when preparing radar images. In this case, however, it was omitted because the spots present on radar imagery can carry important information about building infrastructure. The next step was to generate the GLCM. For Sentinel-1,  $\sigma_0$  images with VH and VV polarisation were used as input. A window size of 9 by 9 pixels was applied, grey levels were counted in all directions and 32 levels of quantisation were specified. A total of 20 derivative images were generated i.e. Contrast, Dissimilarity, Homogeneity, ASM, Energy, MAX, Entropy, Mean, Variance and Correlation. In the next step, a feature space was created by assembling derived images and original backscatter images as a single Layer Stack file.

The first chosen classification method was the RF method. The significance of individual variables was calculated. This allowed for eliminating variables that do not improve the classification result (4 out of 10 for each polarisation). The following 12 derivatives were finally selected: Correlation\_VV, Correlation\_VH, Homogeneity\_VV, Homogeneity\_VH, Contrast\_VV, Contrast\_VH, Energy\_VV, Energy\_VH, Variance\_VV, Variance\_VH,  $\sigma_0$ \_VV and  $\sigma_0$ \_VH (Fig. 2). The last two derivatives were included as they are

primary images and carry information about the intensity of backscattering. The other variables slightly impacted the classification result and were discarded due to the very long computation time. In Figure 2, the differences between the derivatives from the different VH and VV polarisations (top and bottom, respectively) can be observed. The texture varies with the landscape characteristics of the study area and the imagery used. As a result, it is difficult to select appropriate texture indices for image classification (Chen et al. 2004).

Classification with the MD and RF algorithms for 100 and 500 trees was performed. The result of the RF 100 and MD classification with UA polygons is presented in Figure 3. The dominating class is consistent with the denotation on the polygon. There are few cases where a polygon is entirely filled with pixels corresponding to a given class.

A statistical assessment of accuracy was performed using the Congalton method (Congalton, Green 2009) by analysing 30% of all polygons in the UA database. The total accuracy of the classification results does not reach 30%. The value of the *kappa* coefficient indicates a slight agreement between the classification result and the reference data according to the division adopted in Okwuashi et al. (2012). Continuous urban fabric class (CUF) is classified mainly as Port Area (PA), Industrial, commercial, public, military and private units (ICPMAPU), or Discontinuous medium density urban fabric (DMDUF) classes. Classes representing agriculture and forests (Pastures, Arable Land, Forests) interpenetrate each other to a significant extent.

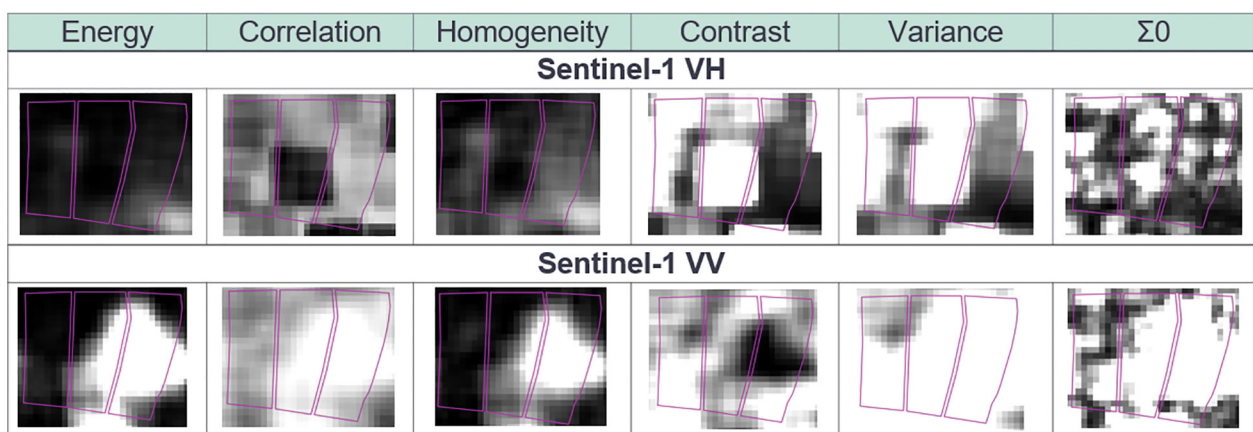


Fig. 2. Sentinel-1 variables selected for classification. The same representative example for the Continuous urban fabric CUF class shown on orthophotomap in Fig. 5.

Class aggregation was performed due to the achieved accuracies in relation to control points. All classes concerning agriculture and forest areas were combined into one class (called 'vegetation'), built-up classes with 30–100% of impermeable areas were aggregated into dense urban areas, built-up with up to 30% of impermeable areas, as well as rural areas (Isolated Structures), were aggregated into the low dense urban areas class, and Port areas (PA) and Industrial, commercial, public military and private units (ICPMAPU) were combined into the industrial urban class (Table 2). The reclassification of test fields was performed using a function implemented in *Python*. After class aggregation, clusters are more consistent and there are also fewer individual pixels (Fig. 4).

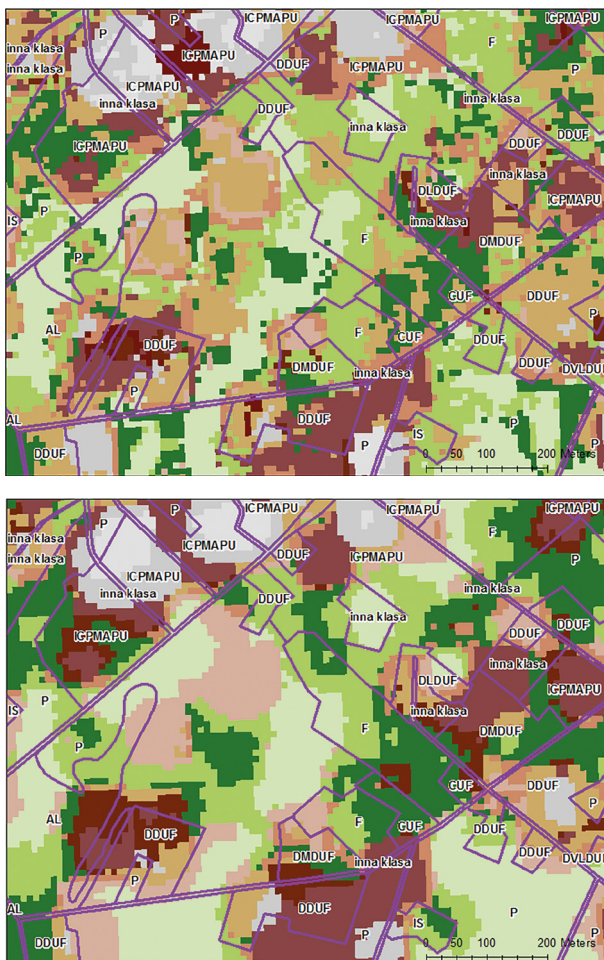


Fig. 3. Results of supervised classification by RF (upper) and MD (lower) for Sentinel-1 with UA class outlines. The fragment shows the representation and variety of different classes in the area. The same legend is applicable as was mentioned in Table 2.

For the MD classification after aggregation, the value of the *kappa* coefficient is 0.47, giving a moderate agreement. The total accuracy of the classification is 64%, which is several percent higher than for RF. The best results were achieved for the vegetation class of almost 80% (P\_Accuracy) and 84% (U\_Accuracy) and industrial built-up areas 56% (P\_Accuracy) and 75% (U\_Accuracy). Studying the classification results pursuant to aggregation, we infer that the classes of vegetation and low density urban areas are largely characterised by a proclivity for being mixed, whereas the class of dense urban areas is frequently mistaken for that of industrial areas (Table 3). The total accuracy of the RF

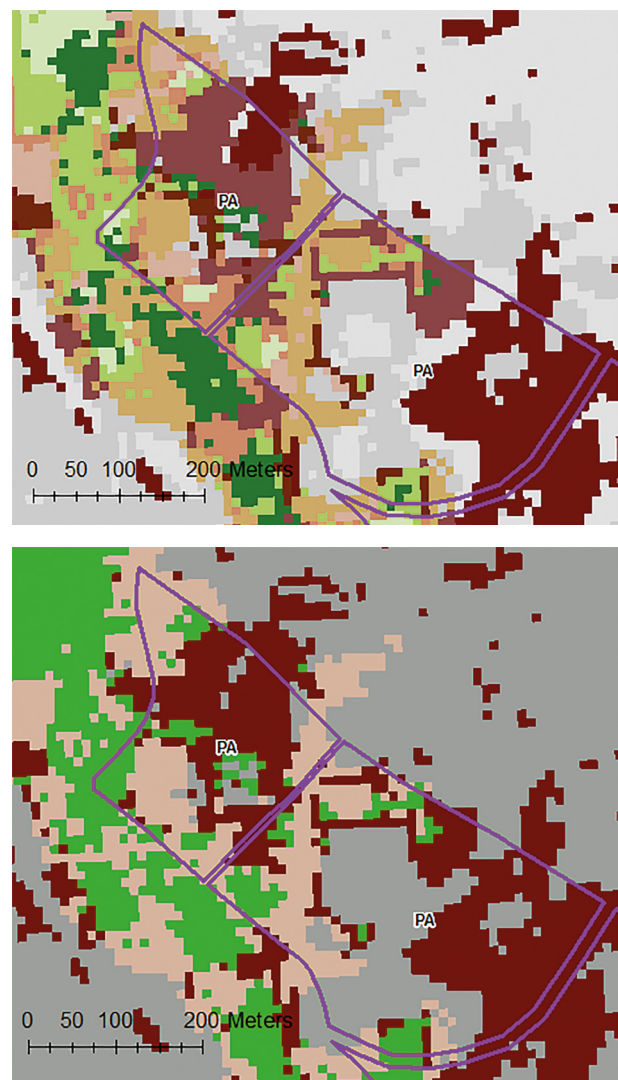


Fig. 4. RF (100 trees) classification result on Sentinel-1 before (upper) and after aggregation to four classes (lower). Example of Port area (PA) class differentiation. The same legend is applicable as was mentioned in Table 2.

Table 3. Sentinel-1 image classification accuracy by RF (top) and MD (bottom) algorithms – both results after aggregation.

Class value	Vegetation	Dense urban	Low dens. urban	Industrial	Total	U_Accuracy	<i>Kappa</i>
	RF classification						
Vegetation	685	58	21	70	834	0.821	0
Dense urban	29	140	5	162	336	0.417	0
Low dens. urban	196	66	17	98	377	0.045	0
Industrial	28	103	2	321	454	0.707	0
Total	938	367	45	651	2001	0	0
P_Accuracy	0.730	0.381	0.378	0.493	0	0.581	0
<i>Kappa</i>	0	0	0	0	0	0	0.398
MD classification							
Vegetation	747	63	21	57	888	0.841	0
Dense urban	32	144	3	118	297	0.485	0
Low dens. urban	141	56	21	114	332	0.063	0
Industrial	18	104	0	362	484	0.748	0
Total	938	367	45	651	2001	0	0
P_Accuracy	0.796	0.392	0.467	0.556	0	0.637	0
<i>Kappa</i>	0	0	0	0	0	0	0.468

classification after aggregation is just over 58%, and the *kappa* coefficient is around 0.4; therefore, the accuracy is almost twice as high, considering the fact that the thematic detail of the classification has been reduced. In summary, the results of the classification of the Sentinel-1 image depended on the defined class contours in the UA. The parametric MD classification method proved to be superior to the non-parametric method, although not all classes were characterised by an increase in accuracy (Table 3).

## ICEYE

For the ICEYE satellite scene in VV polarisation, a radiometric calibration was performed, resulting in an image of backscattering  $\sigma_0$  ( $\sigma_0$ ).

Subsequently, to facilitate data analysis from different sources, a topographic correction was performed to the UTM Zone 34 system using SRTM (3s). The  $\sigma_0$  image had a resolution of 2 m after processing. Next, a GLCM with a window size of  $9 \times 9$  pixels was generated so that the results could be compared with those from Sentinel-1. As input data, the image  $\sigma_0$  in VV polarisation was used, instances of grey levels were counted in all directions, with 32 quantisation levels, and the generation of all possible derived images was set up. As a result of the operation, 10 derivative images were created, and together with the  $\sigma_0$  image, were used to create a feature space consisting of 11 elements (Fig. 5). In case of single polarised VV ICEYE image, all texture measures were used for classification.

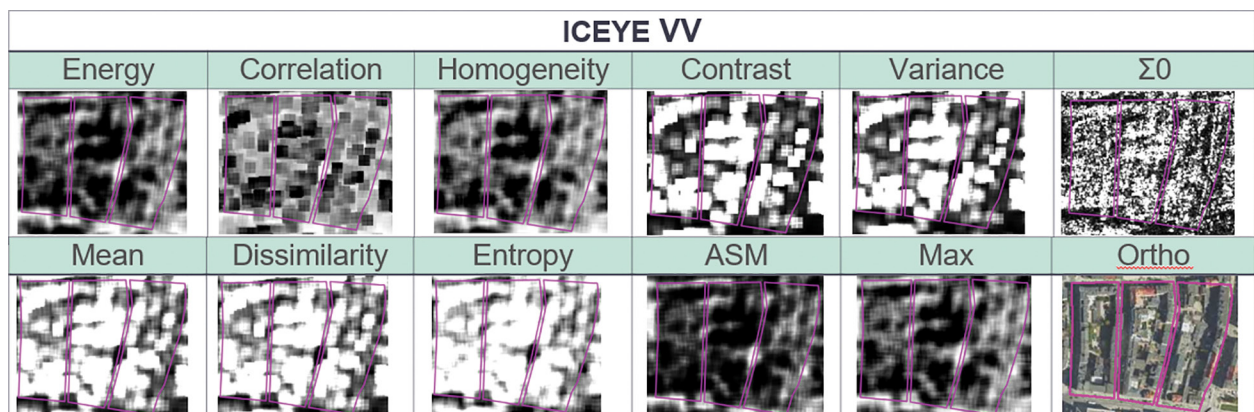


Fig. 5. ICEYE variables selected for classification and contours of the Continuous urban fabric CUF class (as a representative example). The right-bottom orthophoto shows the scale and shape of features.

Based on the same training fields as in the case of the Sentinel-1 classification, statistics were analysed within the reference polygons on all images. Considering the recommendations for multi-layer feature space (Braun and Saulgau 2019), all images, i.e. 11 images in VV polarisation, were used in the classification employing the RF and MD algorithms. The RF algorithm classification on 11 texture images and 11 land use classes was performed on 100 trees. Figure 6 shows the result of the RF and MD classifications – there is a very large fragmentation of classes and Discontinuous low density urban fabric (DLDUF) is the dominating class. Some clusters of pixels depicting built-up area are limited to individual buildings and, as a rule, all colours other than the dominant one correspond to buildings, excluding those clusters located in pasture or forest areas.

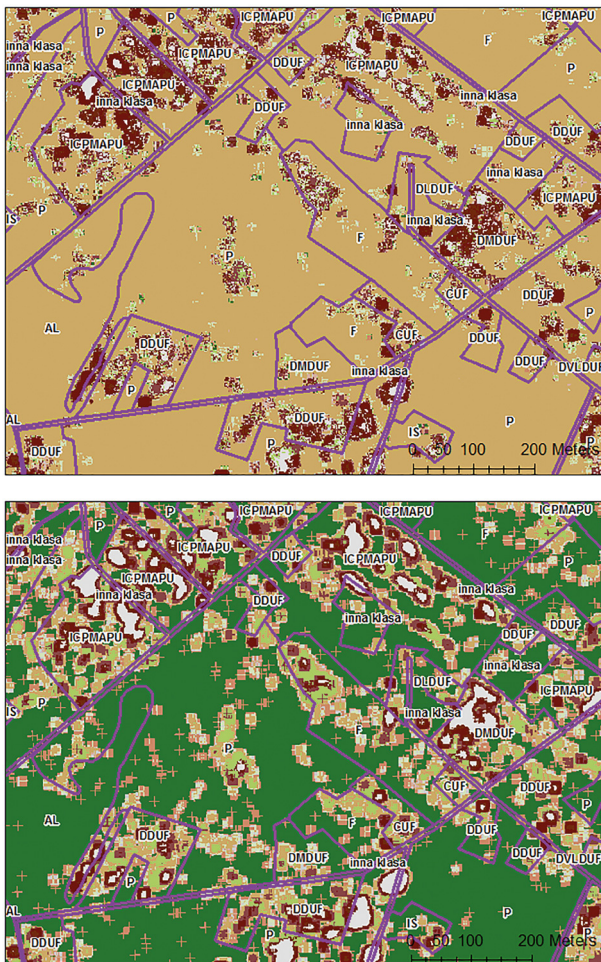


Fig. 6. Results of classification using RF (upper) and MD (lower) on ICEYE image with UA class borders.

The same legend is applicable as was mentioned in Table 2. This representative example shows the diversity of classes.

The accuracy assessment performed on the same test points as for Sentinel-1 confirms what could be noticed by visually analysing a fragment of the image (Fig. 6). Given the accuracy of the classification of less than 5% and the value of the *kappa* coefficient of 0.011, the correspondence between the classification and the reference is small; thus, it is practically impossible to rely on it. From the error matrix it can be deduced that in the case of ICEYE data, Continuous urban fabric (SL >80%) was classified mainly as Discontinuous dense urban fabric (SL: 50–80%), Discontinuous medium density (SL: 30–50%) and Port Area. A dominance of the Discontinuous low density urban fabric (SL: 10–30%) class in the classification is also visible. Similarly, as for Sentinel-1 data, the Industrial, commercial, public, military and private units class is also quite scattered. Probably the biggest difference from the result of the Sentinel-1 classification is the incorrect distinction between vegetation classes and the Discontinuous low density urban fabric (DLDUF) class (Fig. 6).

Class aggregation was performed in the same way as for Sentinel-1 data, and thus, again four classes were created: Dense urban area, Low density urban area, Industrial area and Vegetation. The improvement in accuracy with respect to RF results can be observed by analysing the values from Table 4. In the case of classification with the MD algorithm, the excess of the DLDUF class has been significantly reduced. The total accuracy of the RF classification is 10% higher up to 51%, and the *kappa* coefficient also increased slightly to a value of 0.28. The reclassification of classes improved the readability of the image (Fig. 8). The areas marked with brown and grey colour

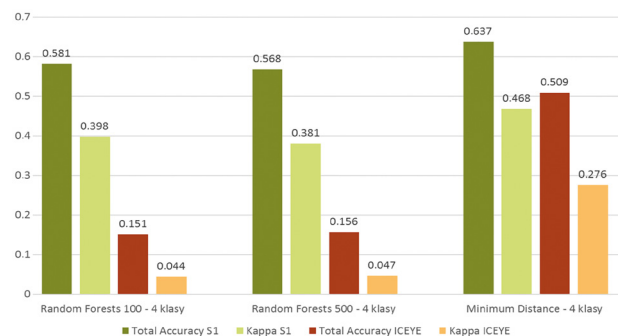


Fig. 7. Overall classification accuracy (total and *kappa*) based on RF and MD classifiers for Sentinel-1 (S1, in green colours) and ICEYE (brown-orange colours).

Table 4. ICEYE image classification accuracy by RF (top) and MD (bottom) algorithms – both results after aggregation.

Class value	Vegetation	Dense urban	Low dens. urban	Industrial	Total	U_Accuracy	<i>Kappa</i>
	RF classification						
Vegetation	50	34	4	63	151	0.331	0
Dense urban	33	148	3	261	445	0.333	0
Low dens. urban	846	125	34	246	1251	0.027	0
Industrial	9	60	4	81	154	0.526	0
Total	938	367	45	651	2001	0	0
P_Accuracy	0.053	0.403	0.756	0.124	0	0.156	0
<i>Kappa</i>	0	0	0	0	0	0	0.047
MD classification							
Vegetation	744	77	25	194	1040	0.715	0
Dense urban	11	110	4	179	304	0.362	0
Low dens. urban	163	71	13	127	374	0.035	0
Industrial	20	109	3	151	283	0.534	0
Total	938	367	45	651	2001	0	0
P_Accuracy	0.793	0.300	0.289	0.232	0	0.509	0
<i>Kappa</i>	0	0	0	0	0	0	0.276

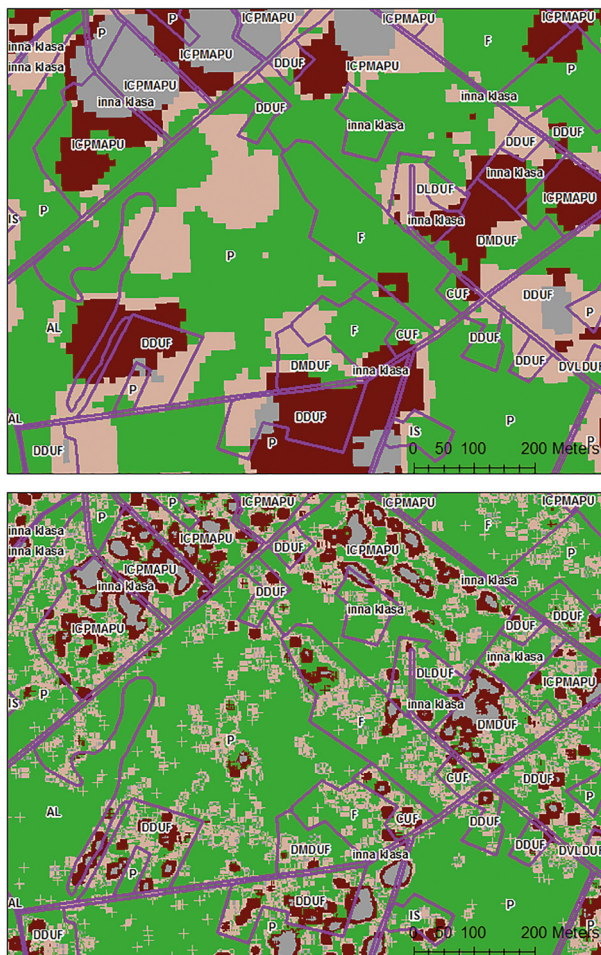


Fig. 8. Comparison of Sentinel-1 (upper) and ICEYE (lower) results based on MD classifier, after class aggregation. The same legend is applicable as was mentioned in Table 2. This representative example shows the diversity of classes.

i.e. dense and industrial urban areas usually correspond to built-up classes in the UA database. Low density urban area is mostly confused with vegetation class. In the ICEYE classification images, there are no cases of polygons majorly filled with only one class, and thus the correct classification of built-up area classes for this type of data is difficult.

## Discussion

The accuracy assessment was carried out on 2000 points evenly distributed in the test polygons. The best accuracy was achieved for the Sentinel-1 image with MD algorithm, 64%, and for ICEYE, 51%. Deploying the RF classification with, variously, 500 and 100 trees produces similar values for accuracy, as can be inferred from the fact of there being no significant difference in the results (Fig. 7).

When visualising the classification results it can be observed that there are no polygons clearly classified as one class defined in UA, although in Sentinel-1 images the dominant class in polygons very often corresponds to their actual function. Nevertheless, the spatial structure of buildings itself is better reproduced in the ICEYE image (Fig. 8). Within most of the contours, there were at least two classes identified, and their occurrence next to each other had a logical justification. Images representing aggregated classes can

Table 5. Comparison of classification results in different images and different algorithms for Continuous urban fabric class and discontinuous dense urban fabric, both in one dense urban area class; these representative examples visualise a general pattern.

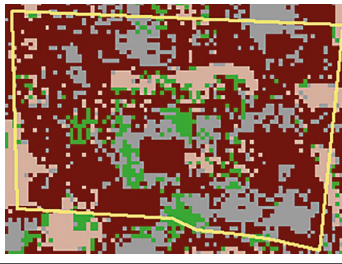
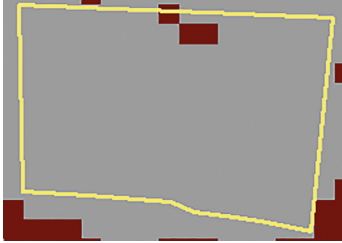
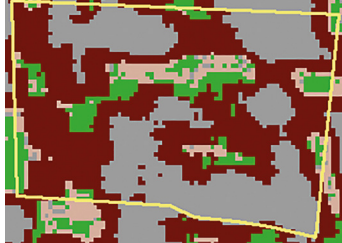
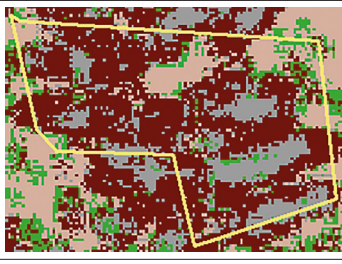
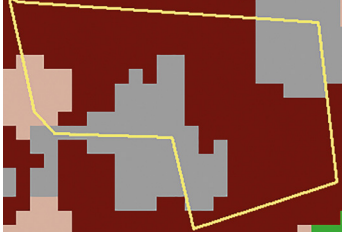
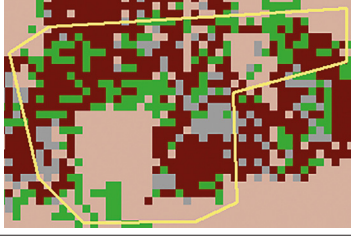
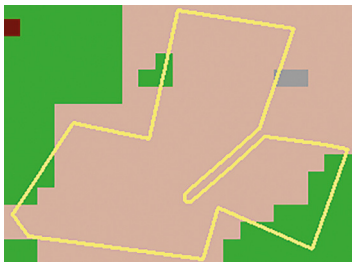
Continuous urban fabric		
orthophotomap		<ul style="list-style-type: none"> <li><span style="display: inline-block; width: 15px; height: 15px; background-color: #800000; border: 1px solid black; margin-right: 5px;"></span> Dense urban area</li> <li><span style="display: inline-block; width: 15px; height: 15px; background-color: #A08080; border: 1px solid black; margin-right: 5px;"></span> Low density urban area</li> <li><span style="display: inline-block; width: 15px; height: 15px; background-color: #808080; border: 1px solid black; margin-right: 5px;"></span> Industrial area</li> <li><span style="display: inline-block; width: 15px; height: 15px; background-color: #008000; border: 1px solid black; margin-right: 5px;"></span> Vegetation</li> <li><span style="display: inline-block; width: 15px; height: 15px; border: 2px solid yellow; margin-right: 5px;"></span> Urban Atlas feature</li> </ul>
	Sentinel-1	ICEYE
Random Forests		
Minimum Distance		
Discontinuous dense urban fabric		
orthophotomap		
	Sentinel-1	ICEYE
Random Forests		
Minimum Distance		

Table 6. Comparison of classification results in different images and different algorithms for discontinuous low and very low density urban fabric, both in low density urban area class; these representative examples visualise a general pattern.

Discontinuous low density urban fabric		
orthophotomap		<ul style="list-style-type: none"> <li><span style="display: inline-block; width: 15px; height: 15px; background-color: #800000; margin-right: 5px;"></span> Dense urban area</li> <li><span style="display: inline-block; width: 15px; height: 15px; background-color: #A08060; margin-right: 5px;"></span> Low density urban area</li> <li><span style="display: inline-block; width: 15px; height: 15px; background-color: #808080; margin-right: 5px;"></span> Industrial area</li> <li><span style="display: inline-block; width: 15px; height: 15px; background-color: #008000; margin-right: 5px;"></span> Vegetation</li> <li><span style="display: inline-block; border: 1px solid yellow; width: 15px; height: 15px; margin-right: 5px;"></span> Urban Atlas feature</li> </ul>
	Sentinel-1	ICEYE
Random Forests		
Minimum Distance		
Discontinuous very low density urban fabric		
orthophotomap		
	Sentinel-1	ICEYE
Random Forests		
Minimum Distance		

be used to analyse and validate the assignment of classes to polygons, or as an aid in creating a database in a new area.

The classification results of Sentinel-1 and ICEYE images differ from each other. Tables 5 and 6 present and visualise a set of processing results. It should be noted that pixel size directly related to wavelength is significant in distinguishing objects. For shorter X-waves (ICEYE), there is more field detail. For C-waves (Sentinel-1), the classes are more averaged and thus correspond better to the class definitions in the UA (also compare Figs 2 and 5). In the case of dense urban area, it is difficult to distinguish individual objects because they overlap and merge into larger clusters. Some of the classes defined in UA database are impossible to classify correctly because of their function, rather than physical characteristics. This applies to the following: Port Areas (PA) and Industrial, Commercial, Public, Military and Private Units (ICPMAPU), as well as Isolated structures and Discontinuous low or very low density urban fabric. Only in some cases can the arrangement of buildings be distinguished, and this applies to low dense urban classes in ICEYE images. It can be observed that the ICEYE images turned out to be too detailed for this application and do not corresponding directly to UA classes' definition (Tables 5 and 6).

The classification results are due to the adopted training and control fields directly emergent from the UA database. The polygons representing the particular contours were developed by interpretation and therefore often the subjective vision of the database operator. Even if one estimated the density of buildings correctly, the boundary could still be drawn at one's discretion, which was also evident through comparison with aerial orthophotos. Although supervised classification did not show a high efficiency in distinguishing classes according to built-up density, it nevertheless seems that texture analysis supports such a process. Sentinel-1 performed better than ICEYE, with its texture images better complementing the features of urban area classes. Automatic acquisition of training fields directly from UA is problematic in terms of obtaining reference data for built-up area categories.

This remains a significant challenge due to the complexity of urban areas in defining and characterising urban area classes. Tables 5 and 6 show

the differences in classification results in the images from the two sensors corresponding to UA classes shown on the orthophotos.

## Conclusions

Although radar images reflect the spatial structure of buildings, this trait did not impact the results of the classification according to density of built-up area. The high resolution of the ICEYE data led to a relatively low accuracy of the classification of built-up area classes. For this reason, the ICEYE data turned out to be too detailed for this application and could probably be used in other cases to classify individual objects. It is also worth noting that each polarisation highlights different elements of objects and their spatial structure. Thus, through employing more polarisation combinations, a more complete characteristic of objects can be obtained based on Sentinel-1.

The starting point for the classification should be the physical objects in the field, rather than the UA polygons of land use or land cover. In case of Sentinel-1, the dominant class in the polygon reflected reality and corresponded to the label in the UA database. The automatic acquisition of training and control fields from the UA is problematic and does not guarantee high performance of the results. It is therefore advisable to obtain reference data for test areas on one's own.

The non-parametric method of classification - RF - in this case did not work well and gave weaker classification results than the parametric MD method. In the case of classes after aggregation for Sentinel-1 and ICEYE, the use of the MD algorithm allowed accuracies of 64% and 51%, respectively, to be achieved. Hence, the use of the MD algorithm avoids significant errors in classification. The aggregation of classes is a good move towards further analysis for grey infrastructure density within urban zones. The results of the classification itself are a good input layer for analysing the density of grey infrastructure. This is still a significant challenge due to the complexity of buildings (shape, size, orientation, distribution) and their surroundings (road, open area, etc.) in automatically distinguishing and classifying built-up area classes. A contextualised approach could also be used to identify the density-based classes.

## Acknowledgements

To Michał Kossakowski for the support in the text translation. The authors thank the reviewers for valuable comments that improved the final version of the paper. Additionally, the authors would like to thank ICEYE and ESA for making SAR data available for free through an open access platform.

## Author contributions

Conceptualization and methodology, JPK; formal analysis, data curation and visualization, JG; resources investigation, JPK; writing – original draft preparation, JG; writing – review and editing, JPK; supervision, JPK. All authors have read and agreed to the published version of the manuscript.

## Funding

This research received no external funding.

## References

- BIP [Biuletyn Informacji Publicznej], 2021. Biuletyn Informacji Publicznej Urzędu Miasta Gdyni. Online: [bip.um.gdynia.pl](http://bip.um.gdynia.pl) (accessed 8 July 2021).
- Braun A., Hochschild V., 2015. *Combining SAR and optical data for environmental assessments around refugee camps*. Eberhard Karls University, Tybinga.
- Braun A., Saulgau B., 2019. *Radar satellite imagery for humanitarian response. Bridging the gap between technology and application*. Eberhard Karls University, Tybinga.
- Breiman L., 2001. Random forests. *Machine Learning* 45(1): 5–32.
- Breiman L., Cutler A., 2021. Online: [https://www.stat.berkeley.edu/~breiman/RandomForests/cc\\_home.htm](https://www.stat.berkeley.edu/~breiman/RandomForests/cc_home.htm) (accessed 14 February 2021).
- Chen C.H., 2008. *Image processing for remote sensing*. Taylor & Francis Group Boca Raton: 39–106, 341–354.
- Chen D., Stow D.A., Gong P., 2004. Examining the effect of spatial resolution and texture window size on classification accuracy: An urban environment case. *International Journal of Remote Sensing* 25(11): 2177–2192. DOI 10.1080/01431160310001618464.
- Clausi D.A., 2002. An analysis of co-occurrence texture statistics as a function of grey level quantization. *Canadian Journal of Remote Sensing* 28(1): 45–62.
- Congalton R.G., Green K., 2009. *Assessing the accuracy of remotely sensed data: Principles and practices*. 2nd edn. Lewis Publishers, Boca Raton.
- Creodias Finder. Online: <https://finder.creodias.eu/> (accessed 2 March 2021).
- Dell'Acqua F., Gamba P., 2003. Texture-based characterisation of urban environments on satellite SAR images. *IEEE Transactions on Geoscience and Remote Sensing* 41(1): 153–159.
- Denis M., 2018. Selected issues regarding small compact city – Advantages and disadvantages. *Space and Form* 34: 151–162. DOI 10.21005/pif.2018.34.C-03.
- Eckardt R., Urbazaev M., Salepci N., Pathe C., Schmillius Ch., Woodhouse I., Stewart Ch., 2021. *Echoes in Space. Introduction to Radar Remote Sensing*. SAR MOOC Manuscript, EO-College.org, ESA, EOS. Friedrich-Schiller-University of Jena. Online: [https://eo-college.org/resource/urban\\_lc/](https://eo-college.org/resource/urban_lc/) (accessed 03 September 2021).
- GHSL [Global Human Settlement Layer], 2022. Urban footprint. Online: <https://ghsl.jrc.ec.europa.eu/> (accessed 19 December 2022).
- Giannini M.B., Merola P., Allegrini A., 2012. Texture analysis for urban areas classification in high resolution satellite imagery. *Applied Remote Sensing Journal* 2(2): 65–71.
- Goodman J.W., 1976. Some fundamental properties of speckle. *Journal of the Optical Society of America* 66(11): 1145–1150.
- Hall-Beyer M., 2017a. *GLCM texture: A tutorial v. 3.0*. Department of Geography, University of Calgary.
- Hall-Beyer M., 2017b. Practical guidelines for choosing GLCM textures to use in landscape classification tasks over a range of moderate spatial scales. *International Journal of Remote Sensing* 38(5): 1312–1338.
- Haralick R.M., Shanmugam K., Dinstein I., 1973. Textural features for image classification. *IEEE Transactions on Systems, Man, and Cybernetics* 3: 610–621.
- Herold M., Goldstein N.C., Clarke K.C., 2003. The spatiotemporal form of urban growth: Measurement, analysis and modeling. *Remote Sensing of Environment* 86(3): 286–302. DOI 10.1016/S0034-4257(03)00075-0.
- Holobacă I.-H., Ivan K., Alexe M., 2019. Extracting built-up areas from Sentinel-1 imagery using land-cover classification and texture analysis. *International Journal of Remote Sensing* 40: 8054–8069.
- Huang X., Zhang T., 2020. Morphological building index (MBI) and its applications to urban areas. In: Weng Q., Quattrochi D., Gamba P. (eds), *Urban remote sensing*. 2<sup>nd</sup> edition Taylor & Francis Group Boca Raton: 33–49.
- ICEYE Specification. Online: <https://www.iceye.com/satellite-missions> (accessed 2 March 2021).
- Joelsson S.R., Benediktsson J.A., Sveinsson J.R., 2008. Random forest classification of remote sensing data. In: Chen C.H. (ed.), *Image processing for remote sensing*. Taylor & Francis Group: 61–78.
- Kamusoko C., 2022. *Optical and SAR remote sensing of urban areas. A practical guide*. Springer: 71–103.
- Kupidura P., 2015. *Application of image granulometry to classification of satellite images*. Publishing House of Warsaw University of Technology, Warsaw.
- Kupidura P., 2019. The comparison of different methods of texture analysis for their efficacy for land use classification in satellite imagery. *Remote Sensing* 11(10): 1233. DOI 10.3390/rs11101233.
- Kupidura P., Uwarowa I., 2017. The comparison of GLCM and granulometry for distinction of different classes of urban area. In: 2017 *Joint Urban Remote Sensing Event (JURSE)*. IEEE. DOI 10.1109/JURSE.2017.7924615.
- Lewiński S., Aleksandrowicz S., 2012. Evaluation of usability of texture in identifying basic land cover classes on the satellite images of different resolutions. *Archiwum Fotogrametrii, Kartografii i Teledetekcji* 23: 229–237.
- Mohanaiah P., Sathyanarayana P., Gurus Kumar L., 2013. Image texture feature extraction using GLCM approach.

- International Journal of Scientific and Research Publications* 3(5): 1–5.
- Molch K., 2009. *Radar earth observation imagery for urban area characterizations*. JRC Scientific and Technical Reports, European Communities, Luxembourg.
- Okwuashi O., Isong M., Eyo E., Eyoh A., Nwanekezie O., Olayinka D.N., Udoudo D.O., Ofem B., 2012. GIS cellular automata using artificial neural network for land use change simulation of Lagos, Nigeria. *Journal of Geography and Geology* 4(2): 94–101.
- Park Y., Guldmann J.-M., 2020. Measuring continuous landscape patterns with gray-level co-occurrence matrix (GLCM) indices: An alternative to patch metrics? *Ecological Indicators* 109: 105802, DOI 10.1016/j.ecolind.2019.105802.
- Pathak V., Dikshit O., 2010. A new approach for finding an appropriate combination of texture parameters for classification. *Geocarto International* 25: 295–313.
- Richards J.A., 2013. *Remote sensing digital image analysis. An introduction*, 5th edn. Springer-Verlag Berlin Heidelberg: 247–315, 381–433.
- SDG [Sustainable Development Goals], 2015. Goals/Tasks 11.1.1 and 11.3.1. 2022. Online: <https://sdgs.un.org/goals/goal11> (accessed 23 May 2022).
- Semenzato A., Pappalardo S.E., Codato D., Trivelloni U., De Zorzi S., Ferrari S., De Marchi M., Massironi M., 2020. Mapping and monitoring urban environment through sentinel-1 SAR data: A case study in the Veneto Region (Italy). *ISPRS International Journal of Geo-Information* 9: 375. DOI 10.3390/ijgi9060375.
- Sentinel-1 Specification. Online: <https://sentinels.copernicus.eu/web/sentinel/user-guides/sentinel-1-sar/data-formats/safe-specification> (accessed 2 March 2021).
- Snitkowska E., 2004. Analiza tekstur w obrazach cyfrowych i jej zastosowanie do obrazów angiograficznych – rozprawa doktorska. *Politechnika Warszawska, Wydział Elektroniki i Technik Informacyjnych, Instytut Automatyki i Informatyki Stosowanej*.
- Urban Atlas Database. Online: <https://land.copernicus.eu/local/urban-atlas> (accessed 2 March 2021).
- Urban Atlas Guide. Online: <https://land.copernicus.eu/user-corner/technical-library/urban-atlas-mapping-guide> (accessed 2 March 2021).
- Wellmann T., Haase D., Knapp S., Salbach C., Selsam P., Lausch A., 2018. Urban land use intensity assessment: The potential of spatio-temporal spectral traits with remote sensing. *Ecological Indicators* 85: 190–203.
- Yoshioka M., Fujinaka T., Omatu S., 2008. SAR image classification by support vector machine. In: Chen C.H. (ed.), *Image processing for remote sensing*. Taylor & Francis Group: 341–353.
- Zhang Q., Wang J., 2001. Texture analysis for urban spatial pattern study using SPOT imagery. In: *Proceedings IEEE International Geoscience and Remote Sensing Symposium: 2149–2151*. 9–13 July 2001, University of New South Wales, Sydney, Australia.